Rapid, biochemical tagging of cellular activity history in vivo

Run Zhang[1,2], Maribel Anguiano[2,3], Isak K. Aarrestad[2,3,4], Sophia Lin[2], Joshua Chandra[2,3], Sruti S. Vadde[2], David E. Olson[2,4,5,6], Christina K. Kim[2,4,7]*

[1]Biomedical Engineering Graduate Group, University of California, Davis, Davis, CA 95616
[2]Center for Neuroscience, University of California, Davis, Davis, CA 95618
[3]Neuroscience Graduate Group, University of California, Davis, Davis, CA 95618
[4]Institute for Psychedelics and Neurotherapeutics, University of California, Davis, Davis, CA 95616
[5]Department of Chemistry, University of California, Davis, Davis, CA 95616
[6]Department of Biochemistry and Molecular Medicine, University of California, Davis, Sacramento, CA 95817
[7]Department of Neurology, University of California, Davis, Sacramento, CA 95817

***Corresponding author:** tinakim@ucdavis.edu

ABSTRACT
Intracellular calcium (Ca^{2+}) is ubiquitous to cell signaling across all biology. While existing fluorescent sensors and reporters can detect activated cells with elevated Ca^{2+} levels, these approaches require implants to deliver light to deep tissue, precluding their noninvasive use in freely-behaving animals. Here we engineered an enzyme-catalyzed approach that rapidly and biochemically tags cells with elevated Ca^{2+} in vivo. Ca^{2+}-activated Split-TurboID (CaST) labels activated cells within 10 minutes with an exogenously-delivered biotin molecule. The enzymatic signal increases with Ca^{2+} concentration and biotin labeling time, demonstrating that CaST is a time-gated integrator of total Ca^{2+} activity. Furthermore, the CaST read-out can be performed immediately after activity labeling, in contrast to transcriptional reporters that require hours to produce signal. These capabilities allowed us to apply CaST in a new context to tag prefrontal cortex neurons activated by psilocybin, and to correlate the CaST signal with psilocybin-induced head-twitch responses in untethered mice.

MAIN TEXT
Dynamic changes in intracellular ion concentrations allow cells to respond and adapt to their local environment, ultimately contributing to the normal physiological functioning of organisms. For example, neurons which are the basic functional units of the brain, can be activated by various external stimuli or pharmacological compounds, leading to rapid fluctuations in intracellular calcium ion (Ca^{2+}) concentrations. Thus, the activity among complex neural networks can be measured using cellular changes in Ca^{2+} levels as a direct proxy for neuronal firing. Genetically-encodable Ca^{2+} indicators have transformed our ability to record neural activity in awake and behaving animals[1-4]. However, a major limitation of fluorescent sensors is that their read-out is transient, and they generally require invasive methods to gain optical access to deep brain structures. This can make it challenging to couple the activity history of a given neuron with its numerous other cellular properties (e.g., precise spatial localization, RNA expression, or protein expression).

To overcome this issue, previous efforts have focused on designing orthogonal transcriptional reporters (FLARE[5], FLiCRE[6], Cal-Light[7]) or fluorescent proteins (CaMPARI[8]) that can stably mark activated cells undergoing high intracellular Ca^{2+}. However, these approaches implement light-sensitive proteins that require blue[9] or UV[10] light in order to restrict the time window of activity labeling in cells. As with fluorescent sensors, this requirement significantly hampers their scalability in deep brain regions, or in body areas where fibers for light delivery cannot be implanted. Alternative stable tagging approaches include immediate early gene (IEG)-based transcriptional reporters (TRAP[11], TRAP2[12, 13], and tetTag[14, 15]), which utilize a drug injection instead of light to gate the activity labeling window. However, while IEG activity has generally been linked to neural activity in many cell-types[16], it is not nearly as universal a read-out as Ca^{2+} is. Furthermore, the slow onset of IEG expression limits the ability to immediately tag and identify neurons activated during a specific time window. This is compounded by the fact that all transcription-based activity reporters take several hours (~6-18 hrs[6, 17]) before sufficient levels of the reporter protein can be detected. Thus, there is a need for a completely new strategy that enables non-invasive and rapid activity-dependent labeling of cells.

Here we envisioned designing an activity-dependent enzyme that can attach a small, biochemical handle to activated cells exhibited high intracellular Ca^{2+}. Our strategy was to re-engineer and re-purpose a proximity-labeling enzyme, split-TurboID[18], to report increased intracellular Ca^{2+} in living cells by tagging proteins with an exogenously delivered biotin molecule. Proximity labeling enzymes such as split-TurboID[18] (and its predecessors, BioID[19] and TurboID[20]) have been traditionally used to biotinylate statically expressed proteins for downstream enrichment and analysis over long periods (typically 4-7 days in vivo). But they

have not been engineered to detect dynamic changes in intracellular ion concentrations in vivo. Our design, CaST (Ca^{2+}-activated Split-TurboID), enzymatically tags activated neurons within brief, user-defined time windows of exogenous biotin delivery. The biotinylated proteins can then immediately be read-out using any existing method for biotin-detection. Since the biotin molecule is both cell- and blood brain barrier-permeable, this facilitates its application in living organisms.

RESULTS

Design and optimization of a Ca^{2+}-activated Split-TurboID (CaST).

The basic CaST design tethers the Ca^{2+}-binding protein calmodulin (CaM) and a CaM-binding synthetic peptide M13 variant to either inactive half of split-TurboID (**Fig. 1A**). We postulated that under high cytosolic Ca^{2+} concentrations, the CaM fragment would be recruited to M13, resulting in the reconstitution and activation of split-TurboID. Upon simultaneous biotin supplementation, the reconstituted split-TurboID would then biotinylate itself, and nearby proteins, in a Ca^{2+}-dependent manner. High Ca^{2+} alone should not result in signal, as the endogenous biotin levels are too low to result in substantial protein biotinylation; and exogenous biotin alone should not result in signal, as the split-TurboID inactive fragments remain separated (**Fig 1B**). Thus, CaST can act as a coincidence detector of both exogenous biotin and high intracellular Ca^{2+}.

Initially, we tested various approaches to tether CaM and M13 to either of the split-TurboID fragments, sTb(N) and sTb(C). Four different versions of the tool were transfected into HEK293T cells, with different conformational arrangements and different subcellular localizations of the proteins (**Supplementary Fig. 1A**). Cells were treated with a combination of biotin with or without Ca^{2+} and an ionophore for 30 minutes, and then fixed and stained for biotinylated proteins using Streptavidin conjugated to Alexa-647 (SA-647). Both the GFP and SA-647 fluorescence were quantified for each cell and were ratioed to normalize for expression levels (SA-647/GFP). Importantly, all four versions had no SA-647 signal in the absence of exogenously delivered biotin. Of the four versions, we found that a membrane-tethered CD4-sTb(C)-M13-GFP with a cytosolic CaM-V5-sTb(N) resulted in the highest signal-to-background ratio (SBR) of biotin ± Ca^{2+} tagging (**Supplementary Fig. 1B**). We subsequently designated this optimized construct as our final CaST design (**Fig. 1B**). Western blot analysis confirmed that CaST-transfected HEK239T (CaST-HEK) cells treated with biotin and Ca^{2+} for 30 minutes exhibited elevated biotinylation signal compared to CaST-HEK cells treated with negative control conditions (**Fig. 1C,D**). Immunohistochemistry and confocal imaging showed that both fragments of the tool are expressed in HEK cells, confirming that the low SA-647 signal in negative control conditions is not due to a lack of fragment co-expression (**Fig. 1E**). However, purposefully omitting either fragment of CaST in the presence of biotin and Ca^{2+} resulted in no biotinylation signal, as expected (**Supplementary Fig. 2A**).

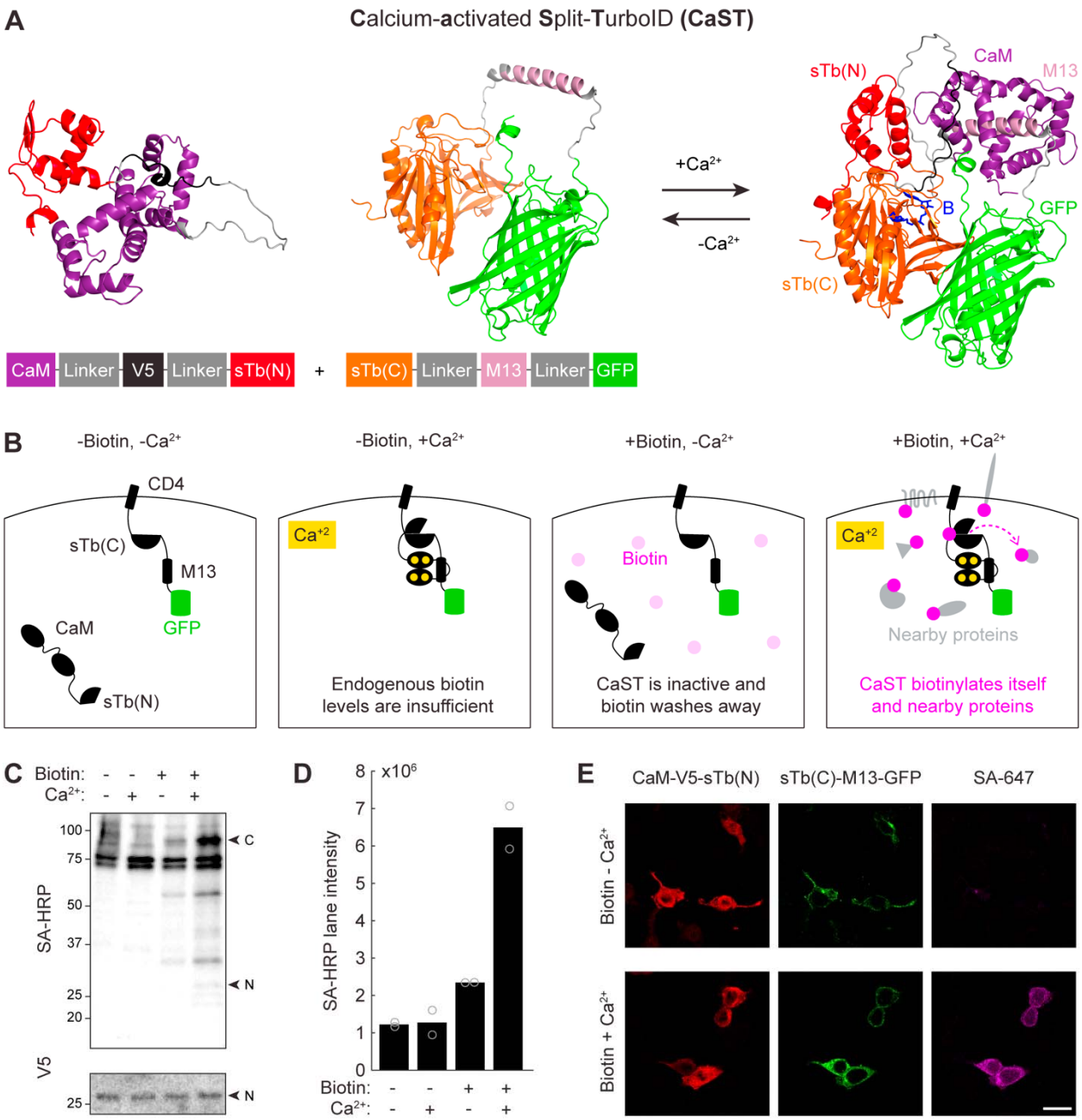

Figure 1. Design of a Ca^{2+}-activated Split-TurboID (CaST).
A) AlphaFold2[21, 22] prediction of the CaST protein structures in the absence (left) and presence (right) of high Ca^{2+}. The two CaST components reversibly reconstitute in a Ca^{2+}-dependent manner. The predicted biotin binding site is shown in blue.
B) Schematic of CaST design for expression in HEK cells. The component with sTb(C)-M13-GFP is tethered to the membrane via CD4, while the CaM-sTb(N) component is expressed throughout the cytosol. CaST only tags proteins when cells are treated with biotin and exhibit elevated intracellular Ca^{2+}.
C) HEK cells were transfected with CaST and treated with ± 50 µM biotin and ± Ca^{2+} (5 mM $CaCl_2$ and 1 µM ionomycin) for 30 minutes. Cells were then washed with DPBS, and whole-cell lysates were collected and analyzed using a Western blot stained with streptavidin-Horse Radish Peroxidase (SA-HRP) or anti-V5/HRP. "N" indicates the expected size of the CaM-V5-sTb(N) fragment, while "C" indicates the expected size of the CD4-sTb(C)-M13-GFP fragment.

D) Quantification of biotinylated proteins present in Western blot lanes of the experiment shown in panel **C**. Two independent biological replicates were quantified.
E) Example confocal images of HEK cells transfected with both components of CaST and treated with biotin ± Ca^{2+} for 30 minutes, as described in panel **C**. Cells were washed, fixed, and stained with anti-V5 and streptavidin-AlexaFluor647 (SA-647). The anti-V5 signal stains the CaM-sTb(N) component (left), while the GFP fluorescence shows the CD4-sTb(C)-M13 component (middle). Cells treated with high Ca^{2+} exhibit robust biotinylation of proteins, detected by SA-647 staining (right). Scale bar, 20 µm.

Quantification and characterization of CaST labeling in HEK cells

To further quantify the extent of biotin- and Ca^{2+}-dependent CaST labeling, we performed fluorescence imaging across multiple fields of views (FOVs) in CaST-HEK cells treated with biotin with or without Ca^{2+} for 30 minutes (**Fig. 2A**). Single cell analysis confirmed that the Ca^{2+}-dependent increase in SA-647 labeling was present across cells with varying GFP expression levels of the enzyme, showing that it is not due to differences in expression levels of the tool across conditions (**Fig. 2B**). The distributions of normalized SA-647/GFP fluorescence also differed significantly between cells treated with or without Ca^{2+} (**Fig. 2C**). These results demonstrate that CaST robustly detects elevated intracellular Ca^{2+} levels in living cells.

To optimize CaST delivery, we concatenated its two fragments into a bi-cistronic vector containing either a porcine teschovirus 2A peptide (P2A) coding sequence or internal ribosome entry sites (IRES). P2A and IRES are well-established strategies for co-expressing multiple proteins from a single promoter[23, 24], ensuring that each cell expresses both fragments of CaST. We found that both CaST-P2A and CaST-IRES exhibited higher SA-647/GFP labeling with biotin and Ca^{2+} compared to with biotin alone (**Supplementary Fig. 2B**). We chose to further characterize the CaST-IRES version, as it resulted in a higher biotin ± Ca^{2+} SBR (5-fold, compared to 2.7-fold; **Supplementary Fig. 2B**). As with the non-IRES version, CaST-IRES exhibited a Ca^{2+}-dependent increase in SA-647/GFP labeling across individual cells (**Fig. 2D-G**). Furthermore, in a direct comparison to the non-IRES version, CaST-IRES resulted in lower background SA-647/GFP labeling in cells treated with only biotin, likely due to more controlled protein expression levels of the two components (**Fig. 2H**).

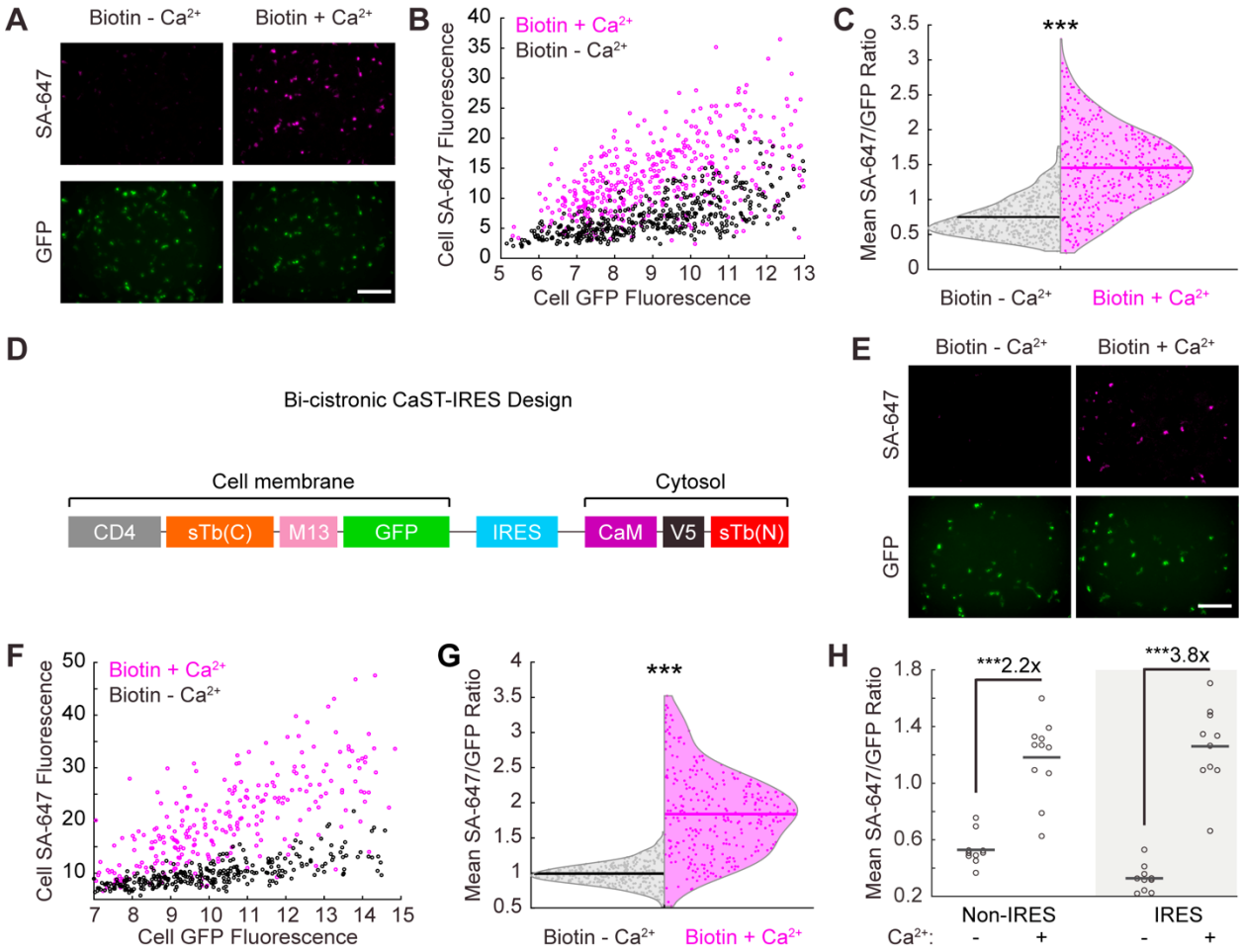

Figure 2. Quantification of CaST's performance.
A) Example 10x FOV images of HEK cells transfected with CaST and treated with 50 µM biotin ± Ca^{2+} (5 mM $CaCl_2$ and 1 µM ionomycin) for 30 minutes. The top row shows SA-647 staining of biotinylated proteins. The bottom row shows expression of the CD4-sTb(C)-M13-GFP component. Scale bar, 300 µm. **B)** Scatter plot of the mean SA-647 versus mean GFP fluorescence calculated for every GFP+ cell detected across 11 FOVs treated with either biotin + Ca^{2+} (n = 451 cells) or biotin - Ca^{2+} (n = 473 cells). **C)** Violin plots showing the distributions of the mean SA-647/GFP fluorescence ratio per cell from data in panel **B**. The mean SA-647/GFP ratio for cells treated with Ca^{2+} was significantly higher than that of cells treated without Ca^{2+} (***P < 0.001, U = 27234, Mann-Whitney U test). **D)** Schematic of the bi-cistronic CaST-IRES construct design. **E)** Example 10x FOV images of HEK cells transfected with CaST-IRES and treated with biotin ± Ca^{2+} for 30 minutes, as in panel **A**. Scale bar, 300 µm. **F)** Scatter plot of the mean SA-647 versus mean GFP fluorescence calculated for each GFP+ cell detected across 10 FOVs treated with either biotin + Ca^{2+} (n = 293 cells) or with biotin - Ca^{2+} (n = 332 cells). **G)** Violin plots showing the distributions of the mean SA-647/GFP fluorescence ratio per cell from data in panel **F**. The mean SA-647/GFP ratio for cells treated with Ca^{2+} was significantly higher than that of cells treated without Ca^{2+} (***P < 0.001, U = 6732, two-tailed Mann-Whitney U test). **H)** The FOV averages of the SA-647/GFP fluorescence ratio per cell from the non-IRES data shown in panel **B**, and the IRES data shown in panel **F**. The non-IRES version exhibited a Ca^{2+}-dependent SBR of 2.2x (n = 11 FOVs per condition; ***P < 0.001, U = 2, two-tailed Mann-Whitney U test). The Ca^{2+}-dependent SBR for the IRES version was 3.8x (n = 10 FOVs per condition; ***P < 0.001, U = 0, two-tailed Mann-Whitney U test).

Temporal resolution and Ca^{2+}-sensitivity of CaST.

Thus far we have demonstrated that CaST requires both biotin and Ca^{2+} delivery to result in robust labeling. However, one important requisite of our design is that both the Ca^{2+}-sensing and split-TurboID reconstitution be reversible. This is so that enzymes activated during high Ca^{2+} prior to the desired biotin labeling window can split back into inactive fragments once the cytosolic Ca^{2+} returns to resting levels. To test for the reversibility of CaST, we treated HEK cells expressing CaST-IRES with Ca^{2+} for 30 minutes, washed the cells over the course of 10 minutes, and then delivered biotin for 30 minutes. We directly compared this condition to CaST-HEK cells treated with biotin alone, or with biotin and Ca^{2+}, for 30 minutes. Cells treated with biotin after removal of Ca^{2+} exhibited no biotinylation, similar to the negative control (**Fig. 3A,B**). This demonstrates that CaST has a temporal resolution for detecting intracellular Ca^{2+} on the order of 10 minutes (meaning it can ignore Ca^{2+} events that occur 10 minutes prior to the desired biotin labeling window).

Next, we asked whether the CaST signal is correlated to the levels of intracellular Ca^{2+} present in cells. We conducted a Ca^{2+} titration experiment in which we treated cells with increasing concentrations of $CaCl_2$ in the media (along with 1 µM ionomycin) and biotin for 30 minutes. Our results demonstrated elevated SA-647/GFP labeling with as low as 2.5 mM $CaCl_2$, that increased in magnitude as the extracellular concentration was raised to 10 mM $CaCl_2$ (**Fig. 3C**). The CaST SA-647/GFP signal was approximately linearly correlated to Ca^{2+} concentration over this range (**Fig. 3D**). These results demonstrate that CaST acts as an integrator of Ca^{2+}.

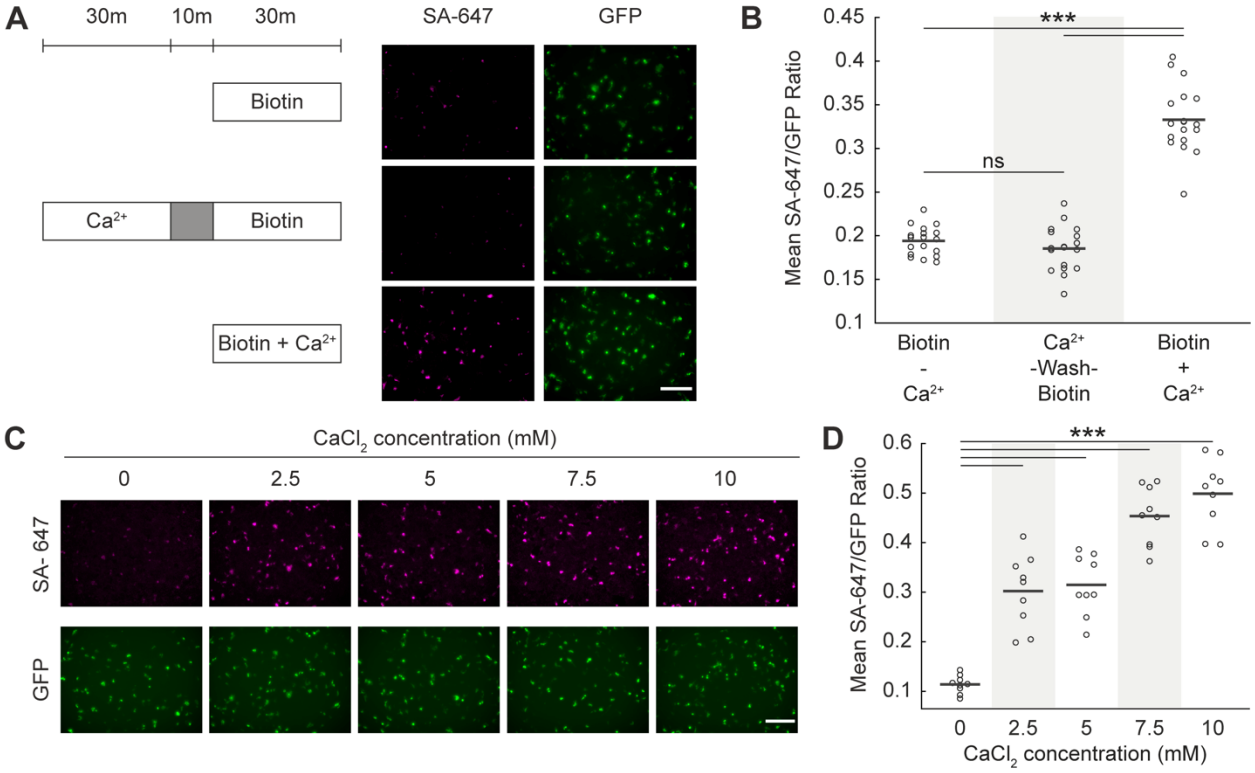

Figure 3. Characterization of reversibility and Ca^{2+} sensitivity of CaST.

A) To test the split enzyme's reversibility, HEK cells were transfected with CaST-IRES and treated either with biotin alone for 30 minutes (top), with Ca^{2+} for 30 minutes followed by a 10-minute wash and then biotin for 30 minutes (middle), or with biotin + Ca^{2+} simultaneously for 30 minutes (bottom). Example 10x

FOV images are shown for all 3 conditions with SA-647 staining of biotin and GFP expression of CaST-IRES. Scale bar, 300 µm.
B) The FOV averages of the SA-647/GFP fluorescence ratio per cell for the 3 conditions shown in panel **A**. Only the biotin + Ca^{2+} condition had a higher mean FOV SA-647/GFP ratio compared to the other two control conditions (n = 18 FOVs per condition; ***P < 0.001, Tukey's post-hoc multiple comparison's test following a 1-way ANOVA, $F_{2,51}$ = 154.3, P < 0.001; ns P = 0.620).
C) Example FOVs of HEK cells transfected with CaST-IRES and treated with biotin and increasing concentrations of $CaCl_2$ (and 1µM ionomycin). Top row: SA-647 staining of biotin. Bottom row: GFP expression of CaST-IRES. Scale bar, 300 µm.
D) The FOV averages of the SA-647/GFP fluorescence ratio per cell for the $CaCl_2$ concentrations shown in panel **C**. All concentrations of $CaCl_2$ delivered resulted in an increased mean FOV SA-647/GFP ratio compared to the biotin alone condition (n = 9 FOVs per condition; ***P < 0.001, Tukey's post-hoc multiple comparison's test following a 1-way ANOVA, $F_{4,40}$ = 57.68, P < 0.001). The FOV average SA-647/GFP ratios were linearly correlated with $CaCl_2$ concentration (Pearson's correlation coefficient r = 0.9644, P = 0.008).

Direct comparison of the SBR and read-out kinetics of CaST to existing technologies.
Compared to existing Ca^{2+}-dependent integrators, CaST has two major advantages: it is non-invasive (using biotin instead of light), and it acts on rapid timescales (tags cells within minutes rather than hours). We directly compared the performance of CaST against an existing light- and Ca^{2+}-dependent integrator, FLiCRE[6]. FLiCRE works via a protease-mediate release of a non-native transcription factor (e.g., Gal4) in the presence of blue light and Ca^{2+}. This released transcription factor then enters the nucleus to drive expression of a modular reporter gene, such as a fluorescent protein (**Supplementary Fig. 3A**). While it has fast labeling kinetics (it can detect 30-s of blue light and elevated Ca^{2+}), its read-out kinetics are slow, requiring transcription and translation of the reporter gene that can take hours to accumulate. Here we transfected HEK cells with either CaST-IRES or FLiCRE and treated cells for 15 minutes with either biotin with or without Ca^{2+}, or light with or without Ca^{2+}, respectively. We then fixed cells either immediately, 2, 4, 6, or 8 hours after the stimulation, and imaged the reporter expression in each case (SA-647 for CaST, and UAS::mCherry for FLiCRE; **Fig. 4A,B,** and **Supplementary Fig. 3B,C**). Across all time points measured, we observed an increases in CaST SA-647 labeling in conditions treated with biotin and calcium compared to with biotin alone; however, an increase in FLiCRE UAS::mCherry reporter expression was only apparent ~8 hours after the light and Ca^{2+} stimulation (**Fig. 4C,D**). The biotin ± Ca^{2+} and light ± Ca^{2+} SBRs were calculated by normalizing the SA-647 or UAS::mCherry expression against an expression marker for each respective tool (GFP; **Fig. 4E,F**, and **Supplementary Fig. 3D-G**). Note that for the cells treated with biotin and Ca^{2+}, the decrease in the SA-647/GFP ratio over the 8 hours is due to both a decrease in SA-647 signal (protein turnover; **Fig. 4C**), and due to an increase in CaST GFP expression (**Supplementary Fig. 3D,E**). These findings demonstrate that in response to the same Ca^{2+} conditions and labeling time, CaST outperforms FLiCRE both in terms of the SBR of labeling observed, and in terms of the kinetics of activation read-out.

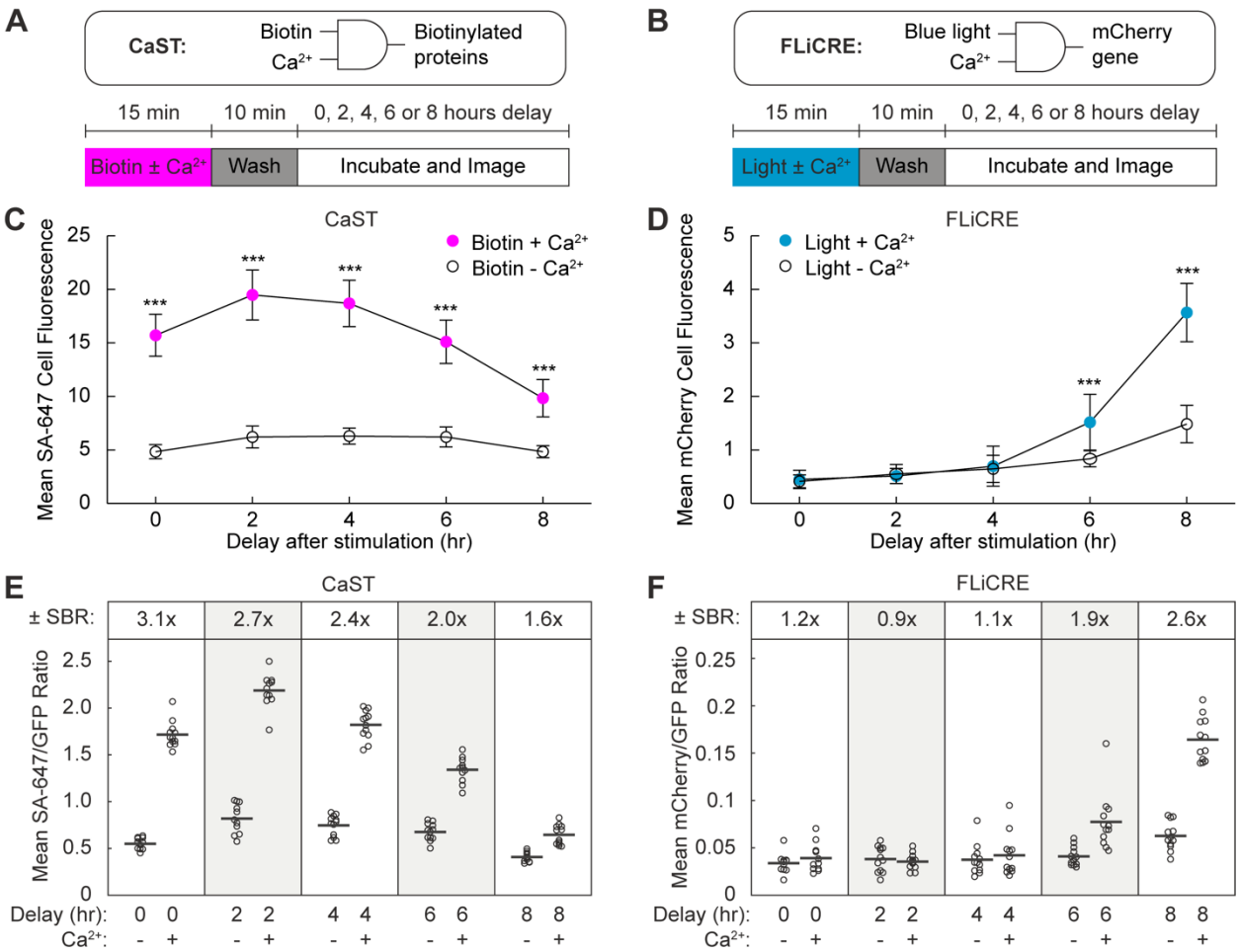

Figure 4. Comparison of CaST to an existing technology, FLiCRE.
A) Schematics of CaST as an AND logic gate, and the experimental paradigm used to test the time course of labeling detection after biotin + Ca^{2+} stimulation. Cells were transfected with CaST-IRES components.
B) Schematics of an existing blue light- and Ca^{2+}-dependent transcriptional reporter, FLiCRE, as an AND logic gate, and the experimental paradigm to test the time course of labeling detection after light + Ca^{2+} stimulation. Cells were transfected with FLiCRE components (**Supplementary Fig. 3A**).
C) For CaST, the FOV average of the SA-647 cell fluorescence was calculated following a variable delay period after biotin ± Ca^{2+} stimulation. The mean SA-647 cell intensity per FOV was significantly greater in the biotin + Ca^{2+} versus biotin - Ca^{2+} condition across all timepoints (n = 11-12 FOVs per condition; ***P < 0.001, Tukey's post-hoc multiple comparison's test following a 2-way ANOVA, $F_{4,108}$ = 25.94, P < 0.0001). Data is plotted as mean ± s.e.m.
D) For FLiCRE, the FOV average of the UAS::mCherry cell fluorescence was calculated following a variable delay period after light ± Ca^{2+} stimulation. The mean mCherry cell intensity per FOV was significantly greater in the light + Ca^{2+} versus light - Ca^{2+} condition only at the 6- and 8-hour timepoints (n = 11-12 FOVs per condition; ***P < 0.001, Tukey's post-hoc multiple comparison's test following a 2-way ANOVA, $F_{4,108}$ = 46.46, P < 0.0001). Data is plotted as mean ± s.e.m.
E, F) The ± Ca^{2+} SBR of normalized reporter expression is shown for both CaST (panel **E**) and FLiCRE (panel **F**). For CaST, the SA-647 fluorescence is divided by the GFP fluorescence. For FLiCRE, the UAS::mCherry fluorescence is divided by the GFP fluorescence.

Application of CaST in cultured neurons.
We then asked whether CaST could detect elevated intracellular Ca^{2+} in cultured rat hippocampal neurons. We expressed the two-component version of CaST using adeno-associated viruses (AAVs) to obtain the maximal expression levels, and stimulated neurons using potassium chloride (KCl) in the presence of biotin for 30 minutes. Immunofluorescence imaging confirmed that CaST robustly tagged activated neurons treated with biotin and KCl, compared to negative control conditions (**Fig. 5A,B** and **Supplementary Fig. 4A**). Stimulation for only 10 minutes was also sufficient to drive significantly elevated CaST labeling (**Fig. 5C,D**). Quantitative analysis of individual neurons expressing CaST showed that ~65% of neurons in a given FOV treated for 30 minutes with biotin and KCl exhibited strong SA-647 labeling (thresholded as described in **Supplementary Fig. 4B**); in contrast, only ~10% of neurons treated with biotin alone exhibited strong SA-647 labeling (grey bars in **Fig. 5E**, and **Supplementary Fig. 4B,C**). In neurons treated for only 10 minutes, ~35% of neurons were strongly labeled in the biotin and KCl condition, while ~10% of neurons were labeled in the biotin alone condition (white bars in **Fig. 5E**).

Lastly, we investigated the potential for CaST to detect elevated intracellular Ca^{2+} in response to physiological stimuli, such as exposure to neuromodulators or pharmacological agents. We treated neurons with biotin and either 10 µM dopamine (DA), or 10 µM 2,5-dimethoxy-4-iodoamphetamine (DOI; a serotonin 5-HT type 2A/C receptor agonist), for 30 minutes. Both dopamine receptors and 5-HT2A receptors are known to be expressed in rat hippocampal neurons[25-27]. Dopamine receptors are either G_i or G_s protein-coupled receptors, while 5-HT2A receptors are G_q protein-coupled receptors[28, 29]. Whereas activation of G_i/G_s protein signaling primarily modulate cAMP with variable effects on intracellular Ca^{2+} levels, G_q protein signaling should directly elevate intracellular Ca^{2+} levels[30, 31]. Accordingly, we found that biotin and dopamine did not significantly increase SA-647 labeling relative to a biotin alone control; however, biotin and DOI drove a significant increase in SA-647 labeling (**Fig. 5F,G**). These results demonstrate that CaST can be applied to reveal differential responses to pharmacological compounds among a population of neurons containing multiple neuronal subtypes and expressing different receptors.

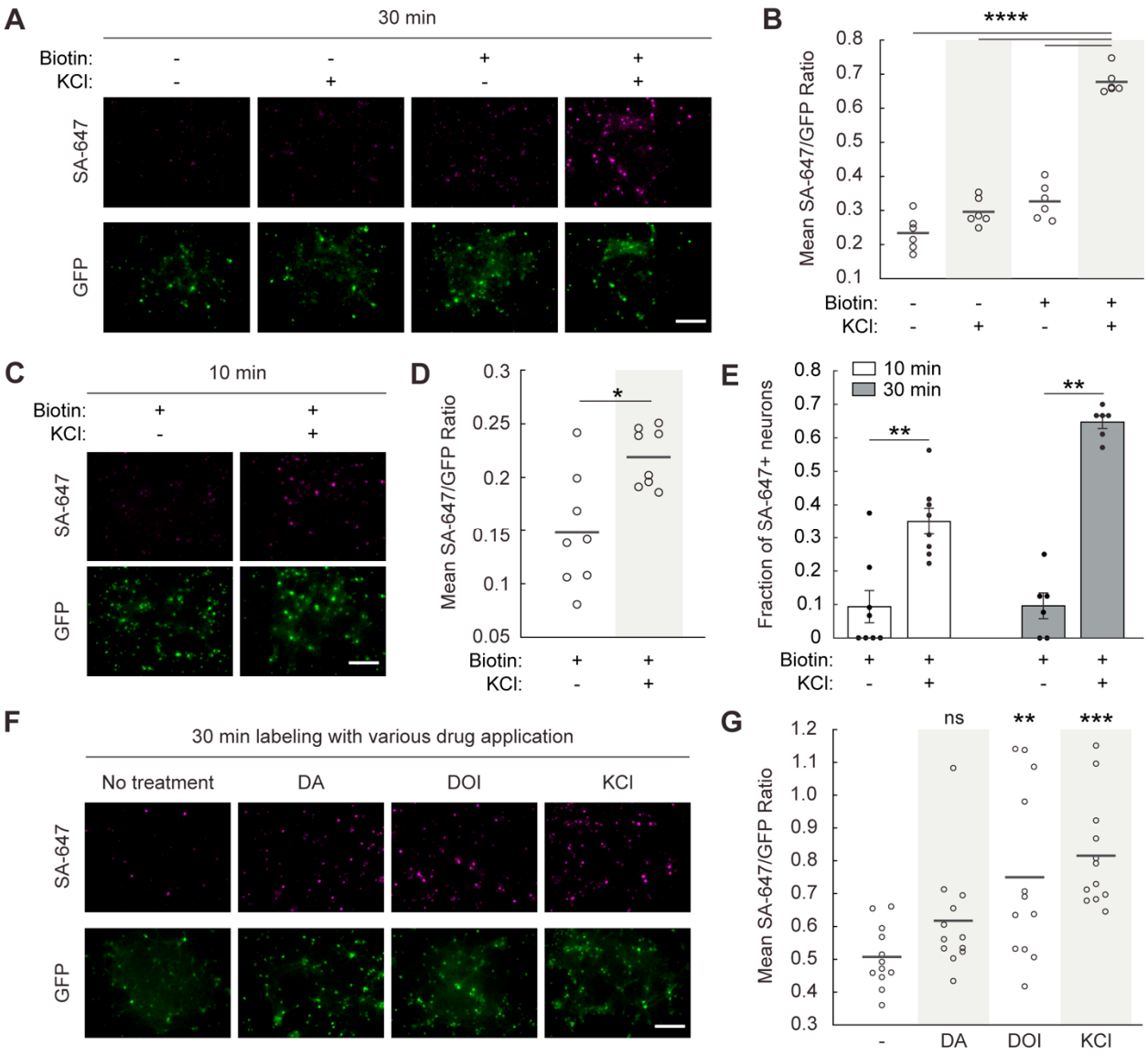

Figure 5. CaST performance in cultured neurons.

A) Example FOVs of cultured rat hippocampal neurons infected with AAV2/1-Synapsin-CD4-sTb(C)-M13-GFP and AAV2/1-Synapsin-CaM-sTb(N) viruses. Neurons were stimulated with 50 µM biotin and 30 mM KCl for 30 minutes, then washed, fixed, and stained for SA-647. Scale bar, 300 µm.

B) The FOV averages of the SA-647/GFP fluorescence ratio per cell for the data shown in panel **A**. The biotin + KCl condition had a greater mean FOV SA-647/GFP ratio compared to all other conditions (n = 6 FOVs per condition; ****P < 0.001, Tukey's post-hoc multiple comparison's test following a 2-way ANOVA, $F_{1,20}$ = 59.43, P < 0.0001). The + biotin - KCl was significantly greater than the - biotin - KCl condition as well (*P = 0.013).

C) Example FOVs of rat hippocampal neurons infected with CaST as in panel **A** but stimulated with biotin ± KCl for only 10 minutes. Scale bar, 300 µm.

D) The FOV averages of the SA-647/GFP fluorescence ratio per cell for the data shown in panel **C**. The mean FOV SA-647/GFP ratio was greater for the biotin + KCl versus biotin - KCl condition (n = 8 FOVs per condition; *P = 0.015, U = 9, two-tailed Mann-Whitney U test).

E) Fraction of all GFP+ neurons that are also strongly SA-647+ (defined as having an SA-647 fluorescence value greater than the 90th percentile of neurons in the biotin - KCl group). Data is quantified

for the 10-minute labeling experiment shown in panel **C** and for a replicated 30-minute labeling experiment shown in **Supplementary Fig. 4B,C**.
F) Example FOVs of rat hippocampal neurons infected with CaST as in panel **A** and treated with 50 µM biotin and 10 µM dopamine (DA), 10 µM DOI, or 30 mM KCl for 30 minutes. Scale bar, 300 µm.
G) The FOV averages of the SA-647/GFP fluorescence ratio per cell for the conditions shown in panel **F** (n = 12 FOVs per condition; ***P < 0.001, **P = 0.008, Tukey's post-hoc multiple comparison's test following a 1-way ANOVA, $F_{3,44}$ = 7.373, P < 0.001; ns P = 0.547).

Rapid identification of psilocybin-activated neurons during untethered behavior in vivo. We next applied CaST in vivo to record cellular activity in behavioral contexts that have previously been challenging to record from with existing methods. Psychedelics are an emerging class of therapeutics that are known to promote neuroplasticity in the prefrontal cortex[32-34] and produce positive behavioral adaptations in animal models of neuropsychiatric disorders[35-38]. These compounds also drive hallucinations in humans; therefore a major pressing area of research is to understand whether the hallucinogenic and therapeutic aspects of psychoplastogens can be decoupled[39]. The main hallucinogenic behavioral correlate of psychedelic drugs in animal models is the head-twitch response (HTR)[40, 41] – a rhythmic rotational head movement that is tightly coupled to 5-HT2A receptor activation and correlated with hallucinogenic potential in humans[41]. Critically, the HTR measurement requires free movement of the animal's head, precluding its measurement in head-fixed rodents under a microscope, or in rodents wearing head-mounted hardware for neuronal recordings. We posited that CaST could be applied to directly correlate cellular neuronal activity with the psychedelic-induced HTR in vivo.

We used CaST to measure how psilocybin, a potent and therapeutically relevant psychedelic, modulates population activity in the medial prefrontal cortex (mPFC) of untethered mice during the simultaneous measurement of the HTR. Notably, there have been conflicting reports as to whether 5-HT2A receptor agonists increase[42-44] or decrease[45, 46] population neuronal activity in the cortex. This could be in part due to the different sensitivities in the previous recording methods used.

We expressed CaST viruses under a pan-neuronal synapsin promoter in the mPFC to unbiasedly identify what percentage of neurons are activated during acute psilocybin injection. Mice expressing CaST were injected with a single intraperitoneal (IP) injection of biotin and saline, or biotin and psilocybin. Mice were video recorded to quantify the number of head-twitches displayed following the drug treatment. 1 hour later, mice were sacrificed, and mPFC slices were stained for SA-647 (**Fig. 6A**). We first asked how psilocybin modulated mPFC neuronal activity using CaST as the read-out. Immunohistochemistry showed an increase in SA-647 labeling in mice treated with psilocybin, compared to control mice treated with saline (**Fig. 6B**). Image quantification showed that individual neurons in psilocybin-treated mice exhibited increased SA-647 fluorescence compared to neurons in saline-treated mice (**Fig. 6C**). The normalized SA-647/GFP cell ratio averaged across FOVs was also significantly elevated in psilocybin- versus saline-treated mice (**Fig. 6D**). CaST identified that ~70% of neurons in the mPFC exhibited strong SA-647 labeling following psilocybin treatment (**Fig. 6E**). Mice not expressing CaST, but injected with biotin and psilocybin, did not exhibit any SA-647 labeling (**Supplementary Fig. 5A,B**).

No prior reports have measured Ca^{2+} activity in the mPFC following psilocybin. Thus, to validate our finding that ~70% of mPFC neurons were activated by psilocybin using CaST, we performed two-photon (2P) scanning microscopy in head-fixed mice. We injected mice in the mPFC with

an AAV encoding the Ca^{2+} indicator GCaMP6f and implanted a 1.0 mm diameter Gradient-Index (GRIN) lens to optically access neurons ~2.5 mm deep in the brain (**Supplementary Fig. 5C**). 2P imaging was conducted in mice immediately after administering saline or psilocybin (**Supplementary Fig. 5D-F**). Similar to our findings with CaST, 2P imaging identified that ~70% of neurons in mPFC were activated by psilocybin (**Supplementary Fig. 5G,H**).

While the 2P GRIN lens imaging validated our CaST findings, this methodology inflicts significant damage to the surrounding tissue, and it also requires head-fixation to record activity. Thus, it is impossible to measure the behavioral HTR during 2P imaging. In contrast, we were able to simultaneously record the HTR during CaST labeling in mice injected with either saline or psilocybin. We then measured the amount of neuronal activity induced in the mPFC as a function of the HTR observed (**Fig. 6F**). The number of SA-647+ neurons was significantly correlated with the number of HTRs measured during the recordings (**Fig. 6G**). The mean SA-647/GFP fluorescence ratio of all neurons was also higher in mice exhibiting psilocybin-induced HTRs (**Fig. 6H**). These results establish CaST as a novel, sensitive technology for rapid and non-invasive tagging of activated neurons in untethered mice.

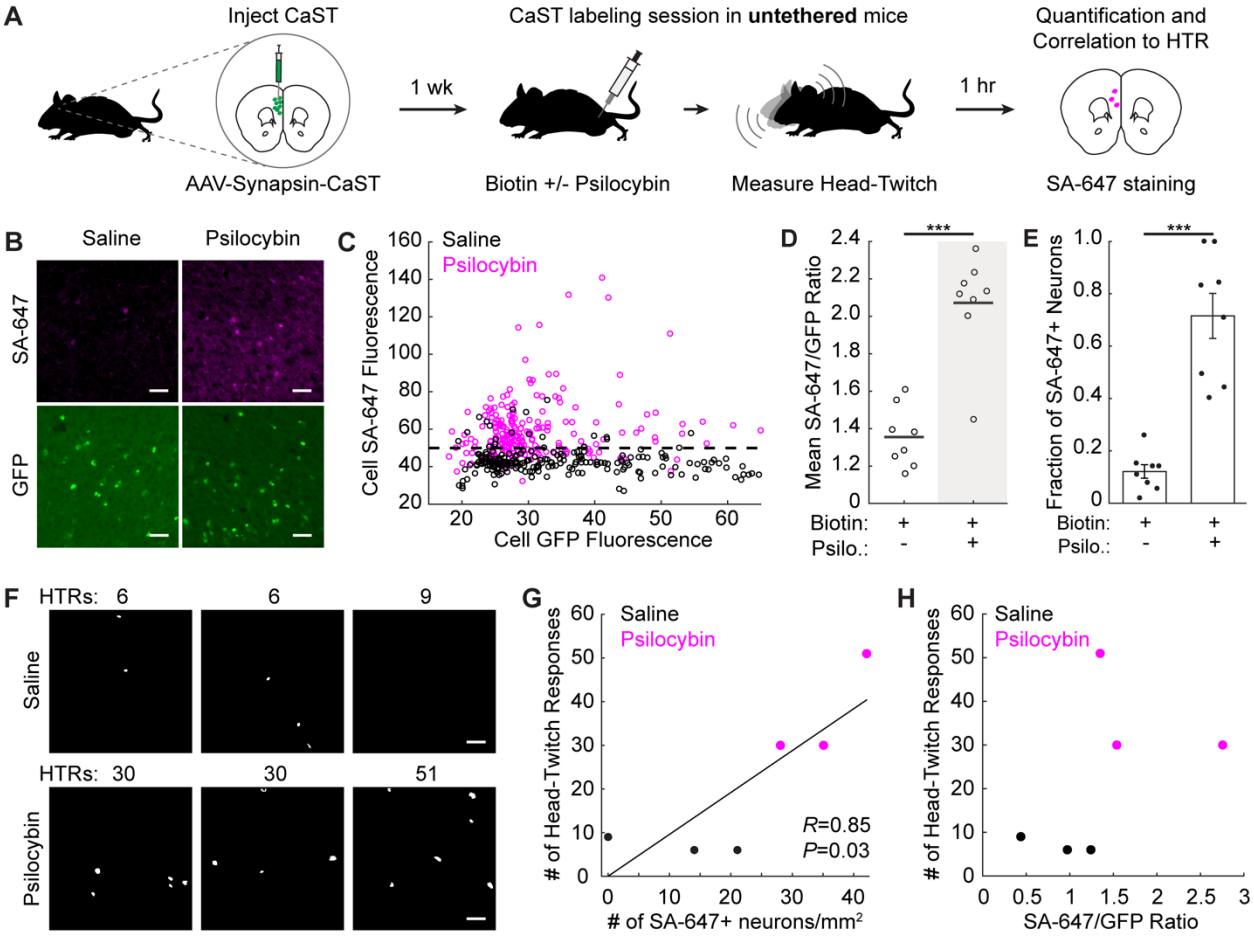

Figure 6. Non-invasive identification of psilocybin-activated neurons in the mPFC during HTR.
A) Schematic for using CaST to tag psilocybin-activated neurons. AAV2/1-Syn-CaST viruses were injected into mPFC. 1 week later, mice were injected with biotin (24 mg/kg) and either saline (5 ml/kg) or psilocybin (3 mg/kg), allowed to explore their cage during HTR measurement, and then sacrificed 1 hour later for histology and quantification.

B) Example epifluorescence images of mPFC slices stained with SA-647 for biotinylated proteins (magenta), and corresponding CaST GFP expression (green), for mice injected with biotin + saline, or biotin + psilocybin. Scale bar, 50 µm.
C) Mean SA-647 versus mean GFP fluorescence calculated for each GFP+ neuron detected in slices from biotin + saline injected mice (black; *n* = 218 neurons from 3 mice) or biotin + saline injected mice (magenta; *n* = 220 neurons from 3 mice). The horizontal dashed line indicates the 90th percentile threshold value of all SA-647 neurons in the biotin + saline group.
D) The FOV averages of the SA-647/GFP fluorescence neuron ratios from panel **I**. The distributions of the two groups different significantly (*n* = 8 FOVs pooled from 3 mice in both conditions; ***P = 6.2e-4, U = 38, two-tailed Mann-Whitney U test).
E) Fraction of all GFP+ neurons that are SA-647+ (thresholded using the dotted line in panel **I**). A larger fraction of neurons were SA-647+ in mice treated with biotin + psilocybin versus mice treated with biotin + saline (*n* = 8 FOVs pooled from 3 mice in both conditions; ***P = 1.6e-4, U = 36, two-tailed Mann-Whitney U test).
F) Cell masks of SA-647+ neurons computationally identified from the mPFC of mice during HTR measurements. The number of head-twitch responses during the first 20 minutes of recording is displayed above each FOV. FOVs with the same number of HTRs were taken from the same mice, but from independent CaST injections on opposite hemispheres. Scale bar, 50 µm.
G) Plot of the number of HTRs versus the number of SA-647+ neurons/mm^2 for *n* = 6 independent CaST injection FOVs shown in panel **F**. The number of HTRs was significantly correlated with the number of SA-647+ neurons (Pearson's correlation coefficient R = 0.85, P = 0.03).
H) Plot of the number of HTRs versus the mean cell SA-647/GFP ratio for the independent CaST injection FOVs shown in panel **F**.

DISCUSSION

Here we demonstrate a new enzymatic approach for stably tagging activated cells with a bio-compatible handle both in vitro and in vivo. Our method, CaST, acts as a Ca^{2+}-dependent ligase, that labels itself and nearby proteins with a biotin tag in living cells. Endogenous biotin levels in cells and in the brain are low enough that CaST requires exogenously delivered biotin in order to robustly tag proteins. Thus, CaST acts as a time-gated integrator of Ca^{2+} concentration, driving the accumulation of biotinylated proteins during a specified labeling period. Importantly, CaST reconstitution is reversible, and following a period of Ca^{2+}-activation, it can be reset to its inactivated state within 10 minutes. Due to its tight temporal resolution and Ca^{2+} sensitivity, CaST was able to robustly detect neurons activated by psilocybin in vivo during the simultaneous measurement of the HTR (which requires freely behaving mice).

CaST reported that approximately 70% of neurons in the prelimbic mPFC are activated by psilocybin in mice. This was corroborated by our own secondary validation studies using single-cell Ca^{2+} imaging. A previous study in rats using in vivo electrophysiology reported that another 5-HT2A receptor agonist, DOI, primarily inhibits mPFC population activity in rats[45]. It is possible that in vivo electrophysiology recordings may be biased towards more highly active neurons at baseline (missing more silent neurons that are activated by psychedelics); or that DOI and psilocybin have different effects on population activity in mPFC. Another recent study using c-Fos labeling following psilocybin injection (1 mg/kg) reported that they could detect elevated c-Fos labeling in the mPFC only when using one of the two different imaging modalities that they tested[44]. This could suggest that the neuronal activity changes driven by psilocybin in the mPFC are challenging to tag using IEG-based approaches and are better detected using Ca^{2+}-based approaches such as CaST.

In contrast to existing light-gated methods for Ca^{2+}-dependent labeling[6, 8, 47], a major advantage of CaST is that it is essentially non-invasive, requiring only the brief injection of a biotin solution

IP in mice which can rapidly cross the blood-brain barrier. This is particularly advantageous in deep tissue, where light must typically be delivered through fiber implantation, significantly limiting the recording area and the range of tool usage. As TurboID can already be used for cell-type-specific biotin proximity labeling across the entire brain[48], it is feasible that CaST can also be scaled as a brain-wide activity-dependent labeling tool in the future, with the use of PhP.eB[49] viruses or transgenic lines. In addition, because the biotin molecule is directly attached to already-expressed proteins, this enables the immediate read-out of activated neurons after the labeling period with CaST. This contrasts with transcriptional-based reporters, including both Ca^{2+}- and IEG-dependent systems, which require multiple hours before activated cells can be easily identified by the reporter RNA or protein. Thus, CaST could be used in cases where it is necessary to tag activated cells and then immediately read-out changes in transcriptional regulation or protein localization without delay.

However, despite the advantages of CaST, it is important to note that the biotin labeling is an "end point experiment" where cells must be fixed and stained for imaging or collected and lysed for protein analysis. Although biotinylated cells can be subjected to subsequent downstream molecular or chemical analysis, proximity labeling itself does not enable further manipulation or genetic access to biotin-tagged neurons. Consequently, CaST is intended to complement, rather than replace, existing tools that can activate induced transcription factors and drive the expression of proteins such as opsins for downstream neuronal manipulation.

Finally, although here we primarily highlight CaST as a novel class of enzymatic-based activity integrators, it is worth noting that it could still be used as a Ca^{2+}-dependent proximity labeling by analyzing biotinylated proteins (see **Fig. 1C**). Thus, future studies could also enrich CaST-tagged proteins for analysis with mass spectrometry to examine activity-dependent differences in subcellular protein expression among unique neuronal cell-types.

METHODS

Cloning

All constructs used or developed in this study are listed in **Supplementary Table 1**. For all constructs, the vectors were double digested with restriction enzymes (New England BioLabs; NEB) following the standard digest protocols. PCR fragments were amplified using Q5 polymerase (NEB). Both vectors and PCR fragments were purified using gel electrophoresis and gel extraction (Qiagen) and were ligated using Gibson assembly (NEB). Ligated plasmids were introduced into NEB Stable Competent *E. coli* (NEB) via heat shock following the manufacture's transformation protocol. Plasmids were amplified using NEB 5-alpha Competent *E. coli* (NEB) and Plasmid Miniprep Kit (Qiagen).

Mammalian cell culture and transfection

Human Embryonic Kidney cell 293T (CRL-3216, ATCC) were cultured as a monolayer in Dulbecco's Modified Eagle Medium (DMEM, Sigma-Aldrich), supplemented with 10% Fetal Bovine Serum (FBS, Sigma-Aldrich) and 1% (v/v) penicillin/streptomycin (P/S, 5,000 U/mL, Life Technologies) (complete DMEM). Cells were cultured in 100 mm TC treated dishes (Falcon) and maintained in the cell culture incubator at 37°C with humidified 5% CO_2 and subcultured when they reached 80%–90% confluence.

For immunofluorescence experiments, cells were plated in 48-well plates pre-treated with 50 mg/mL human fibronectin (Millipore) and incubated for 24 hr. Cells at ~80% confluency were transfected with DNA plasmids using polyethyleneimine max according to the manufacturer's manual (PEI Max, Polysciences). For CaST experiments, cells were transfected with 50 ng

CD4-sTurboID (C)-M13-GFP, 20 ng CaM-V5-sTurboID (N), and 0.8 µL PEI Max per well. For CaST-IRES experiments, cells were transfected with 50 ng CD4-sTurboID (C)-M13-GFP-IRES-CaM-V5-sTurboID (N) and 0.8 µL PEI Max per well. Cells were incubated at 37°C overnight for 15-16 hr prior to stimulation.

For confocal experiments, cells were plated in 35 mm glass bottom dishes (Cellvis) pre-treated with 50 mg/mL human fibronectin (Millipore) and incubated for 24 hr. Cells at ~80% confluency were transfected with DNA plasmids using polyethyleneimine max according to the manufacturer's manual (PEI Max, Polysciences). For CaST experiments, cells were transfected with 250 ng CD4-sTurboID (C)-M13-GFP, 125 ng CaM-V5-sTurboID (N), and 8 µL PEI Max per well. Cells were incubated at 37°C overnight for 15-16 hr prior to stimulation.

HEK293T cell CaST / CaST-IRES experiments

CaST or CaST-IRES HEK cells were stimulated 15-16 hour following transfection. Stimulation master mixes were made by adding $CaCl_2$ (1M stock in H_2O, Sigma), Ionomycin (Sigma), and Biotin (Sigma, B4639; dissolved in DMSO as 100mM stock) to complete DMEM. The stimulation mixtures were then added to the cell and the cells were incubated at 37°C for 30 min for CaST/CaST-IRES labeling. For +Ca^{2+} conditions, we used a final concentration of 5 mM Ca^{2+} and 1 µM Ionomycin. For +biotin conditions, we used a final concentration of 50 µM biotin. After incubation for the indicated time, the solution was removed in each well. Cells were washed once with warm complete DMEM and twice with warm DPBS. Cells were subsequently fixed with 4% (v/v) paraformaldehyde (PFA) in DPBS at room temperature for 10 min followed by two washes with DPBS. After that, cells were permeabilized with ice-cold methanol at -20°C for 8 min followed by two washes with DPBS at room temperature. Cells were incubated with blocking solution (1% w/v BSA, Fisher Scientific, in DPBS) for 45 min at room temperature; followed by a 1 hr incubation in primary antibody solution at room temperature (1:1,000 mouse anti-v5, Invitrogen, R96025). Cells were washed twice with DPBS and incubated with secondary antibody (1:1,000 donkey anti-mouse 568; Abcam, ab175472) and streptavidin-Alexa Fluor647 (1:5,000; Invitrogen, S32357) for 30 min at room temperature. Cells were then washed three times with DPBS and imaged by fluorescence microscopy.

Single fragment CaST experiments were performed by transfecting cells with only one CaST fragment (either 50 ng CD4-sTb(C)-M13-GFP or 20 ng CaM-V5-sTb(N)) or both CaST fragments as positive control. Cells were incubated at 37°C overnight for 15-16 hr prior to stimulation. Stimulation, fixation, and staining were performed as described above.

Reversibility experiments were performed by treating the cells with 5 mM Ca^{2+} and 1 µM ionomycin without biotin at 37°C for 30 min followed by two DPBS washes to wash away Ca^{2+}. Then, the cells were treated with 50 µM biotin without Ca^{2+} for another 30 min. Cells were then fixed and stained as described above.

Ca^{2+} titration experiments were performed by treating the cells with different $CaCl_2$ concentrations ranging from 0 to 10 mM and 1 µM ionomycin at 37°C for 30 min. Cells were then fixed and stained as described above.

HEK293T FLiCRE / CaST-IRES comparison experiment

Transfection of HEK293T cells with FLiCRE was performed as previously described[6]. Briefly, cells were transfected with FLiCRE constructs at ~80% confluency and were immediately wrapped in foil and incubated overnight for 8-9 hr. Transfection of CaST-IRES was performed as described above. On the day of experiment, FLiCRE expressing cells were treated with or without Ca^{2+} and were exposed to blue light simultaneously for a duration of 15 min at 37°C.

The stimulation media containing Ca^{2+} and ionomycin at a final concentration of 6 mM and 1 µM respectively was used to stimulate the FLiCRE expressing cells. For CaST-IRES, cells were treated with biotin ± Ca^{2+} with a final concentration of 5 mM Ca^{2+}, 1 µM ionomycin, and 50 µM Biotin and incubated at 37°C for 15 min. After the stimulation for both CaST-IRES and FLiCRE cells, cells were washed twice with warm DPBS and incubated with DPBS at 37°C for 10 min. After the washes, the DPBS was removed and replaced with 200 µL fresh complete DMEM for further incubation. The cells were fixed either immediately, 2, 4, 6, or 8 hr after the stimulation. Staining was performed after all the cells had been fixed following the methods described above. The biotinylated proteins (SA-647, CaST-IRES) and expression of the reporter (UAS::mCherry, FLiCRE) were imaged using Keyence BZ-X810 fluorescence microscope.

Western blots analysis of CaST

HEK293T cells expressing CaST or CaST-IRES were stimulated and labeled with biotin as described above in 6-well plates and were subsequently washed 3 times with 1 mL DPBS. Cells were then detached from the well by gently pipetting 1 mL of ice-cold DPBS onto the cells and were pelleted by centrifugation at 300 g at 4°C for 3 minutes. The resulted supernatant was removed, and the pellet was lysed on ice for 10 minutes using 100 µL RIPA lysis buffer (50 mM Tris pH 8, 150 mM NaCl, 0.1% SDS, 0.5% sodium deoxycholate, 1% Triton X-100) supplemented with protease inhibitor cocktail (Sigma-Aldrich, P8849) and 1 mM PMSF (G-Biosciences, 82021). The cell lysates were clarified by centrifugation at 13,000 g at 4°C for 10 minutes. The supernatants were collected and mixed with 4x protein loading buffer (PLB). The resulted samples were boiled at 95°C for 10 minutes prior to separation on a 10% precast SDS-PAGE gel. Separated proteins on SDS-PAGE gels were transferred to a nitrocellulose membrane in transfer buffer on ice. The membrane was removed after the transfer and incubated in 5 mL Ponceau stain (0.1% (w/v) Ponceau in 5% acetic acid/water for 5 minutes. The Ponceau stain was then removed with diH_2O and then rinsed with TBST (Tris-buffered saline, 0.1% Tween 20). The membrane was then blocked in 5% (w/v) nonfat dry milk in TBST at room temperature for 1 hour and washed 3 times with TBST for 5 minutes each. To detect biotinylated proteins, the membrane was incubated in 10 mL of 3% BSA/TBST (w/v) with 2 µL streptavidin-HRP (1:5,000; Invitrogen, s911) for 1 hour at room temperature. The blot was washed 3 times with TBST for 5 minutes and was developed with Clarity Max Western ECL Substrate (Bio-Rad) for 1 minute before imaging. To detect the V5 tag, the membrane was incubated in 10 mL of 3% BSA/TBST (w/v) with 1 µL mouse anti-V5 primary antibody (1:10,000; Invitrogen, R96025) for 1 hour at room temperature. The blot was washed 3 times with TBST for 5 minutes and was incubated with 10 mL of 3% BSA/TBST (w/v) with 1 µL anti-mouse-HRP secondary antibody (1:10,000; Bio-Rad, 170-6516) for 30 minutes at room temperature. The blot was washed 3 times with TBST for 5 minutes and was developed with Clarity Max Western ECL Substrate (Bio-Rad) for 1 minute before imaging. The blots were imaged on a Bio-Rad Chemi-Doc XR gel imager. The Western blot images were quantified using ImageJ.

AAV1/2 virus production, concentration, and titration

The production and concentration processes for AAV viruses were conducted following a previously reported method[50, 51]. HEK293T cells at ~80% confluency in 3 T-150 flasks were transfected with 5.2 µg AAV vector, 4.35 µg AAV1 plasmid, 4.35 µg AAV2 plasmid, 10.4 µg DF6 AAV helper plasmid, and 130 µL PEI Max solution per construct and were incubated for 48 hr. After the incubation, the cell culture conditioned media (supernatant) from the T-150 flasks was collected and filtered through 0.45 µm pore size filter (Cytiva) for cultured neuron infection. The remaining HEK293T cells in the flasks were lifted using a cell scraper and were pelleted at 800 g for 10 min for making the purified and concentrated virus. Pelleted cells were then resuspended using 20 mL of 100 mM TBS (100 mM NaCl, 20 mM Tris, pH 8.0). The surfactant, 10% sodium deoxycholate (Sigma-Aldrich), was then added to the resuspended pellet to a final

concentration 0.5%, along with benzonase nuclease (Sigma-Aldrich) to a final concentration of 50 units/mL and incubated for 1 hour at 37°C. Cell debris were removed by centrifugation at 2500 g for 15 minutes and the supernatant was harvested. The clarified cell lysate was loaded to a pre-equilibrated HiTrap heparin column (Cytiva, GE17-0406-01) followed by a 10 mL 100 mM TBS wash using a peristaltic pump, and then successive washes of 1 mL of 200 mM TBS (200 mM NaCl, 20 mM Tris, pH 8.0), and 1 mL of 300 mM TBS (300 mM NaCl, 20 mM Tris, pH 8.0), using a syringe. The bound virus in the column was eluted using a sequence of 1.5 mL 400 mM TBS, 3 mL 450 mM TBS, and 1.5 mL 500 mM TBS (all with 20mM Tris, pH 8.0). Eluted viruses were then concentrated by centrifugation at 2000 g for 2 minutes using a 15 mL centrifugal unit with 100K molecular weight cut off (Amicon) to a final volume of 500 µL. Further concentration of viruses was achieved using a 0.5 mL centrifugal unit (Amicon) to a final volume of 100-200 µL. Titration of the concentrated viruses was performed by AAVpro Titration Kit (for Real Time PCR) Ver.2 (Takara Bio Inc) following the manufacture's protocol. The standard curve was prepared using the positive control solution provided by Takara with serial dilution for absolute quantification. The titer of each viral sample was calculated in reference to the standard curve.

Primary neuronal culture and infection

One day prior to neuron dissociation, 24 well plates and 35 mm glass bottom dishes (Cellvis) were coated with 0.1 mg/mL Poly-D-Lysine (PDL, Millipore Sigma) dissolved in 1X Borate buffer (Fisher Scientific) overnight at room temperature. Plates and dishes were washed four times with sterile diH_2O and dried in the tissue culture hood on the day of neuron dissociation. E18 rat hippocampal tissue (Brain Bits) were dissociated with papain (Brain Bits) and DNase I (Stemcell Technologies) following the manufacturer instructions for neuron dissociation. Dissociated neurons were plated in PDL-coated plates and dishes and cultured in complete Neurobasal Plus medium (Life Technologies) supplemented with 0.01% (v/v) Gentamicin (Life Technologies), 0.75% (v/v) Glutamax (Life Technologies), 2% (v/v) B27 Plus (Life Technologies), 5% (v/v) FBS (Sigma-Aldrich) at 37°C, 5% CO_2. The entire culture medium of each well and dish was removed 24 hr after the plating and replaced with complete Neurobasal Plus medium supplemented with 0.01% (v/v) Gentamicin, 0.75% (v/v) Glutamax, 2% (v/v) B27 Plus to stop glial growth. Subsequently, ~50% of the media in each well was replaced every 3-4 days. At DIV6, neurons were infected with a mixture of crude supernatant of CaST-encoded AAV1/2 viruses by replacing half of the culture media. The plate and dishes were incubated for another ~two weeks in the incubator prior to stimulation.

Primary neuron CaST experiments

Rat hippocampal neurons were dissociated, plated, and infected as described above. At DIV17-22 (~two weeks after infection), neurons were ready for stimulation. Neuron stimulation reagents including Potassium Chloride (KCl), 2,5-dimethoxy-4-iodoamphetamine (DOI; Sigma, D101), and dopamine (DA; Sigma, H8502) were used to introduce neuron firing. A portion of the culture media from each well was taken out and saved in microcentrifuge tubes. The stimulation mixtures were generated by adding the neuron stimulation reagent and biotin solution to the saved culture media to the desired concentration. The stimulation mixtures were then added back to each well and the neurons were incubated at 37°C for 30 min for CaST labeling. For +KCl conditions, we used a final concentration of 30 mM KCl. For +DOI conditions, we used 10 µM of DOI as the final concentration. For +DA conditions, we used a final concentration of 10 µM DA. For +biotin conditions, we used a final concentration of 50 µM biotin. Neurons were then fixed and stained as described above for HEK293T cell experiments. Time series experiments were performed by treating the neurons with or without 30 mM KCl for 10 min or 30 min at 37°C.

Neurons were then fixed and stained as described above for HEK293T cell experiments prior to imaging.

Immunofluorescence imaging and analysis

Cells and neurons imaged immediately after fixation and staining. Fluorescence images were taken with Keyence BZ-X810 fluorescence microscope with an 80W metal halide lamp as the fluorescent light source and a PlanApo 10X air objective lens (NA 0.45). Expression of CaST was visualized by GFP using 470/40 nm excitation filter and 525/50 nm emission filter, and Alexa Fluor568 using 545/25 nm excitation filter and 605/70 nm emission filter. Biotinylated proteins were labeled by SA-647 and visualized by 620/60 nm excitation filter and 700/75 nm emission filter. A CCD camera was used to acquire fluorescence images. Images were analyzed by custom scripts in ImageJ and MATLAB.

Where indicated, confocal imaging was performed using a Zeiss LSM 800 confocal microscope (Carl Zeiss) equipped with 488, 561, and 640nm lasers, and a 63x oil immersion objective (NA 1.4). 35 mm glass bottom dishes with a 14 mm micro-well and #1.5 cover glass (0.16mm-0.19mm) were used for high resolution confocal imaging. Fluorescence images were collected with a 512 x 512-pixel resolution and with a pixel dwell time of 1.03 µsec/pixel. Images were acquired using a PMT detector and emission filter ranges of 450–575 nm, 450–640 nm, and 645–700 nm for EGFP, Alexa Fluor568, and Alexa Fluor647 detection, respectively, for best signal. All images were collected and processed using ZEN software (Carl Zeiss).

Mouse animal models

All experimental and surgical protocols were approved by the University of California, Davis, Institutional Animal Care and Use Committee. For CaST experiments, 5-7 week old male and female wild-type C57BL/6J (Jackson Laboratory Strain 000664) mice were used. Mice were group-housed and given *ad libitum* food and water prior to surgery. Mice were maintained on a reverse 12-hour light/dark cycle.

Mouse stereotaxic surgeries

Briefly, mice were maintained under anesthesia with 1.5 – 2% isoflurane and placed in a stereotaxic apparatus (RWD) on a heating pad. The fur on the top of the skull was removed and antiseptic iodine and 70% alcohol were used in alternation to clean the scalp. Sterile ocular lubricant (Dechra) was administered to the eyes of the mice to protect them from drying out. A midline scalp incision was made, and 0.1% hydrogen peroxide was applied to the skull. A craniotomy was made above the injection site. Virus was then injected into the targeted region using a 33 gauge beveled needle (WPI) and a 10 µL Hamilton syringe controlled by an injection pump (WPI). For all surgeries, 1000 nL total of virus were injected into the targeted mPFC brain region (coordinates: ML +/- 0.5, AP +1.98, DV -2.25) at a rate of 150 nL min^{-1}.

For 2-photon imaging surgeries, 1000 nL of AAV5-CaMKIIa-GCaMP6f was injected into mPFC (diluted 1:1 in DPBS; Addgene, 100834-AAV5, 2.2e12 VG/mL titer). A 1-mm diameter GRIN lens (Inscopix) was then implanted above the mPFC (ML +/- 0.5, AP +1.98, DV -2.05). Implants and custom stainless steel headplates were secured to the skull using dental adhesive and cement system (Pentron, C&B metabond). For CaST surgeries, 500 nL of a 1:1 ratio of the two home-made CaST viruses was injected into mPFC (AAV2/1-Syn-CD4-sTb(C)-M13-GFP, 4.85e9 copies/mL; AAV2/1-Syn-CaM-V5-sTb(N), 4.79e9 copies/mL). Once the surgery was completed, the incision was closed with tissue adhesive (GLUture). Mice received a dose of 3.25 mg/kg EthiqaXR for pain recovery and was revived in a new, clean cage placed on a heating pad.

2-photon Ca^{2+} imaging in mice

2-photon Ca^{2+} imaging was performed using a commercial microscope (Bruker, 2P+) and a 16x, 0.8 NA objective (Nikon, MRP07220). A tunable IR femtosecond pulse laser set to 920 nm (Coherent, Discovery TPC) was used for excitation, and fluorescence emission was collected using a GaAsP PMT (Hamamatsu, H10770PB-40). The excitation laser was directed by galvo scanners sampling 512x512 pixels. Each image was captured at 2 Hz. The imaging field of view was 448x448 µm (optical zoom of 2.5x). Data were collected using the PrairieView software and analyzed using Suite2P[52] and custom MATLAB scripts.

CaST experiments in mice

Mice were handled and given USP grade saline (.9%) injections for three consecutive days before biotin labeling. After a week of viral expression, experimental mice were given two injections, one 24 mg/kg intraperitoneal (IP) injection of diluted biotin solution (Sigma, B4639; dissolved in DMSO as a 10 mM stock solution) and one 3 mg/kg IP injection of psilocybin (synthesized as previously described[35]) dissolved in saline. Control mice were injected with biotin solution and saline (5 ml/kg IP). Mice were placed in separated clean cages following the injection and were sacrificed 1 hour after IP injections. A subset of mice was recorded for head twitch data acquisition following injections.

After biotin labeling, mice were perfused with ice-cold PBS, followed by 4% PFA, and brains were collected and stored in 4% PFA overnight at 4°C. The next day, brains were switched out from PFA and stored in PBS until slicing. 60 µm slices were collected from the mPFC and placed in wells with PBS and stored in 4°C. Slices were washed with PBS-T for 2 mins (3x), then blocked in 5% Normal Donkey Serum (Jackson ImmunoResearch) and 0.3% Triton-X (PBS-T) for 1 hour at room temperature. Slices were stained with streptavidin-Alexa647 (1:1000 dilution; Invitrogen, S32357) in 5% NDS/PBS-T for 1.5 hours at room temperature. Slices were washed with PBS-T for 5 mins at room temperature and then mounted with DAPI-Fluoromount-G (SouthernBiotech) to adhere coverslips. 40x images were taken on BZ-810 Keyence fluorescence microscope.

Data analysis

Custom image analysis scripts in MATLAB and ImageJ were used to analyze fluorescence images. Statistical analysis including Mann-Whitney U test, ordinary one-way ANOVA, two-way ANOVA, and Pearson correlation coefficient calculations were performed by GraphPad Prism 9.0 (GraphPad Software). Significance was defined as a *P* value less than 0.05 for the defined statistical test.

DATA AVAILABILITY

There are no restrictions on data availability. Any data that support the findings of this study are available from the corresponding author upon request.

MATERIALS AVAILABILITY

All plasmids and associated DNA sequences generated in this study will be available on Addgene.

CODE AVAILABILITY

Custom MATLAB scripts used to analyze images will be made available upon publication at: https://github.com/kimck/CaST-analysis-scripts.

ACKNOWLEDGEMENTS
We thank A.Y. Ting (Stanford University) for the generous gift of plasmids used as templates in this study. We thank J. Muir (UC Davis) for assistance with GRIN lens surgeries for in vivo mouse imaging. We thank Hunter T. Warren (UC Davis) and Winston L. Chow (UC Davis) for synthesizing psilocybin. This work was supported by a Burroughs Wellcome Fund Career Awards at the Scientific Interface (#1019469, C.K.K.), the Searle Scholars Program (#SSP-2022-107, C.K.K.), the Boone Family Foundation (D.E.O), and the National Institutes of Health (R01GM128997, D.E.O.). R.Z. was supported by a National Science Foundation (NSF) Research Traineeship (NeuralStorm, #2152260). M.A. was supported by an NSF Graduate Research Fellowship Program (#000895154). J.C. was supported by a National Institutes of Health T32 Training Program (UC Davis Learning, Memory and Plasticity Training Program, T32 MH112507).

AUTHOR CONTRIBUTIONS
R.Z. and C.K.K. conceived the tool design and conceptualized the project. R.Z. performed protein engineering, cultured HEK cell and neuron experiments, image analysis, and data quantification. M.A. performed mouse in vivo CaST experiments, with assistance from I.A.K. I.A.K. analyzed CaST head-twitch data. S.L. performed Western blot experiments and generated AAVs for CaST expression. J.A.C. performed GRIN lens surgeries for in vivo mouse imaging and collected 2P imaging data, with assistance from I.A.K. S.S.V. assisted with HEK cell assays characterizing the different versions of CaST. D.E.O. and I.A.K. provided psilocybin along with critical experimental design input for the in vivo GCaMP imaging and CaST labeling during psilocybin injection. R.Z. led the figure preparation with guidance from C.K.K. R.Z. and C.K.K. wrote the manuscript with contributions from all authors.

COMPETING INTERESTS
D.E.O. is a co-founder of Delix Therapeutics, Inc. and serves as the chief innovation officer and head of the scientific advisory board. All other authors declare no other competing interests.

REFERENCES
1. Grynkiewicz, G., Poenie, M. & Tsien, R.Y. A new generation of Ca2+ indicators with greatly improved fluorescence properties. *Journal of biological chemistry* **260**, 3440-3450 (1985).
2. Tian, L. et al. Imaging neural activity in worms, flies and mice with improved GCaMP calcium indicators. *Nature methods* **6**, 875-881 (2009).
3. Chen, T.-W. et al. Ultrasensitive fluorescent proteins for imaging neuronal activity. *Nature* **499**, 295-300 (2013).
4. Inoue, M. et al. Rational design of a high-affinity, fast, red calcium indicator R-CaMP2. *Nature methods* **12**, 64-70 (2015).
5. Wang, W. et al. A light- and calcium-gated transcription factor for imaging and manipulating activated neurons. *Nature Biotechnology* **35**, 864-871 (2017).
6. Kim, C.K. et al. A Molecular calcium integrator reveals a striatal cell type driving aversion. *Cell* **183**, 2003-2019. e2016 (2020).
7. Lee, D., Hyun, J.H., Jung, K., Hannan, P. & Kwon, H.-B. A calcium- and light-gated switch to induce gene expression in activated neurons. *Nature Biotechnology* **35**, 858-863 (2017).
8. Fosque, B.F. et al. Labeling of active neural circuits in vivo with designed calcium integrators. *Science* **347**, 755-760 (2015).

9. Motta-Mena, L.B. et al. An optogenetic gene expression system with rapid activation and deactivation kinetics. *Nature chemical biology* **10**, 196-202 (2014).
10. McKinney, S.A., Murphy, C.S., Hazelwood, K.L., Davidson, M.W. & Looger, L.L. A bright and photostable photoconvertible fluorescent protein. *Nature Methods* **6**, 131-133 (2009).
11. Guenthner, C.J., Miyamichi, K., Yang, H.H., Heller, H.C. & Luo, L. Permanent genetic access to transiently active neurons via TRAP: targeted recombination in active populations. *Neuron* **78**, 773-784 (2013).
12. Allen, W.E. et al. Thirst-associated preoptic neurons encode an aversive motivational drive. *Science* **357**, 1149-1155 (2017).
13. DeNardo, L.A. et al. Temporal evolution of cortical ensembles promoting remote memory retrieval. *Nature neuroscience* **22**, 460-469 (2019).
14. Reijmers, L.G., Perkins, B.L., Matsuo, N. & Mayford, M. Localization of a Stable Neural Correlate of Associative Memory. *Science* **317**, 1230-1233 (2007).
15. Liu, X. et al. Optogenetic stimulation of a hippocampal engram activates fear memory recall. *Nature* **484**, 381-385 (2012).
16. Choi, J.-E., Kim, J. & Kim, J. Capturing activated neurons and synapses. *Neuroscience Research* **152**, 25-34 (2020).
17. Gore, F. et al. Neural representations of unconditioned stimuli in basolateral amygdala mediate innate and learned responses. *Cell* **162**, 134-145 (2015).
18. Cho, K.F. et al. Split-TurboID enables contact-dependent proximity labeling in cells. *Proceedings of the National Academy of Sciences* **117**, 12143-12154 (2020).
19. Roux, K.J., Kim, D.I., Raida, M. & Burke, B. A promiscuous biotin ligase fusion protein identifies proximal and interacting proteins in mammalian cells. *Journal of Cell Biology* **196**, 801-810 (2012).
20. Branon, T.C. et al. Efficient proximity labeling in living cells and organisms with TurboID. *Nature biotechnology* **36**, 880-887 (2018).
21. Mirdita, M. et al. ColabFold: making protein folding accessible to all. *Nature methods* **19**, 679-682 (2022).
22. Jumper, J. et al. Highly accurate protein structure prediction with AlphaFold. *Nature* **596**, 583-589 (2021).
23. Kim, J.H. et al. High cleavage efficiency of a 2A peptide derived from porcine teschovirus-1 in human cell lines, zebrafish and mice. *PloS one* **6**, e18556 (2011).
24. Mountford, P.S. & Smith, A.G. Internal ribosome entry sites and dicistronic RNAs in mammalian transgenesis. *Trends in Genetics* **11**, 179-184 (1995).
25. Gasbarri, A., Sulli, A. & Packard, M.G. The dopaminergic mesencephalic projections to the hippocampal formation in the rat. *Progress in Neuro-Psychopharmacology and Biological Psychiatry* **21**, 1-22 (1997).
26. Yu, Q. et al. Genetic labeling reveals temporal and spatial expression pattern of D2 dopamine receptor in rat forebrain. *Brain Structure and Function* **224**, 1035-1049 (2019).
27. Bombardi, C. Neuronal localization of 5-HT2A receptor immunoreactivity in the rat hippocampal region. *Brain research bulletin* **87**, 259-273 (2012).
28. Gurevich, E.V., Gainetdinov, R.R. & Gurevich, V.V. G protein-coupled receptor kinases as regulators of dopamine receptor functions. *Pharmacological research* **111**, 1-16 (2016).
29. McCorvy, J.D. & Roth, B.L. Structure and function of serotonin G protein-coupled receptors. *Pharmacology & therapeutics* **150**, 129-142 (2015).
30. Neve, K.A., Seamans, J.K. & Trantham-Davidson, H. Dopamine receptor signaling. *Journal of receptors and signal transduction* **24**, 165-205 (2004).
31. Dhyani, V. et al. GPCR mediated control of calcium dynamics: A systems perspective. *Cellular signalling* **74**, 109717 (2020).

32. Ly, C. et al. Psychedelics promote structural and functional neural plasticity. *Cell reports* **23**, 3170-3182 (2018).
33. Vargas, M.V. et al. Psychedelics promote neuroplasticity through the activation of intracellular 5-HT2A receptors. *Science* **379**, 700-706 (2023).
34. Shao, L.-X. et al. Psilocybin induces rapid and persistent growth of dendritic spines in frontal cortex in vivo. *Neuron* **109**, 2535-2544. e2534 (2021).
35. Cameron, L.P. et al. 5-HT2ARs Mediate Therapeutic Behavioral Effects of Psychedelic Tryptamines. *ACS Chemical Neuroscience* (2023).
36. Catlow, B.J., Song, S., Paredes, D.A., Kirstein, C.L. & Sanchez-Ramos, J. Effects of psilocybin on hippocampal neurogenesis and extinction of trace fear conditioning. *Experimental brain research* **228**, 481-491 (2013).
37. Hibicke, M., Landry, A.N., Kramer, H.M., Talman, Z.K. & Nichols, C.D. Psychedelics, but not ketamine, produce persistent antidepressant-like effects in a rodent experimental system for the study of depression. *ACS chemical neuroscience* **11**, 864-871 (2020).
38. Hesselgrave, N., Troppoli, T.A., Wulff, A.B., Cole, A.B. & Thompson, S.M. Harnessing psilocybin: antidepressant-like behavioral and synaptic actions of psilocybin are independent of 5-HT2R activation in mice. *Proceedings of the National Academy of Sciences* **118**, e2022489118 (2021).
39. Cameron, L.P. et al. A non-hallucinogenic psychedelic analogue with therapeutic potential. *Nature* **589**, 474-479 (2021).
40. Corne, S., Pickering, R. & Warner, B. A method for assessing the effects of drugs on the central actions of 5-hydroxytryptamine. *British journal of pharmacology and chemotherapy* **20**, 106-120 (1963).
41. Halberstadt, A.L. & Geyer, M.A. Characterization of the head-twitch response induced by hallucinogens in mice: detection of the behavior based on the dynamics of head movement. *Psychopharmacology* **227**, 727-739 (2013).
42. González-Maeso, J. et al. Hallucinogens recruit specific cortical 5-HT2A receptor-mediated signaling pathways to affect behavior. *Neuron* **53**, 439-452 (2007).
43. Jefsen, O.H., Elfving, B., Wegener, G. & Müller, H.K. Transcriptional regulation in the rat prefrontal cortex and hippocampus after a single administration of psilocybin. *Journal of Psychopharmacology* **35**, 483-493 (2021).
44. Davoudian, P.A., Shao, L.-X. & Kwan, A.C. Shared and distinct brain regions targeted for immediate early gene expression by ketamine and psilocybin. *ACS Chemical Neuroscience* **14**, 468-480 (2023).
45. Wood, J., Kim, Y. & Moghaddam, B. Disruption of prefrontal cortex large scale neuronal activity by different classes of psychotomimetic drugs. *Journal of Neuroscience* **32**, 3022-3031 (2012).
46. Michaiel, A.M., Parker, P.R. & Niell, C.M. A hallucinogenic serotonin-2A receptor agonist reduces visual response gain and alters temporal dynamics in mouse V1. *Cell reports* **26**, 3475-3483. e3474 (2019).
47. Wang, W. et al. A light- and calcium-gated transcription factor for imaging and manipulating activated neurons. *Nature biotechnology* **35**, 864-871 (2017).
48. Rayaprolu, S. et al. Cell type-specific biotin labeling in vivo resolves regional neuronal and astrocyte proteomic differences in mouse brain. *Nature Communications* **13**, 2927 (2022).
49. Chan, K.Y. et al. Engineered AAVs for efficient noninvasive gene delivery to the central and peripheral nervous systems. *Nature neuroscience* **20**, 1172-1179 (2017).
50. Konermann, S. et al. Optical control of mammalian endogenous transcription and epigenetic states. *Nature* **500**, 472-476 (2013).
51. Wang, W. et al. A light-and calcium-gated transcription factor for imaging and manipulating activated neurons. *Nature biotechnology* **35**, 864-871 (2017).

52. Pachitariu, M. et al. Suite2p: beyond 10,000 neurons with standard two-photon microscopy. *BioRxiv*, 061507 (2016).